J Supercond Nov Magn (2014) 27:2097–2103
DOI 10.1007/s10948-014-2555-7

ORIGINAL PAPER

Poly(amidoamine)-Grafted Superparamagnetic Iron Oxide Nanoparticles: Synthesis and Characterization

Umran Kurtan · Sinem Esir · Abdulhadi Baykal · Hüseyin Sözeri

Received: 21 March 2014 / Accepted: 4 April 2014 / Published online: 24 May 2014

Abstract In this study, the surface of amino silane modified magnetite nanoparticles were coated with polyamidoamine dendrimer up to the fifth generation via a modified repetitive Michael addition and amidation processes. Products were characterized with X-ray powder diffractometry (XRD), transmission electron microscopy (TEM), Fourier transform infrared spectroscopy (FT-IR), thermal gravimetry (TG), and vibrating sample magnetometry (VSM) which proved the superparamagnetic properties of all products. The attachment of silane group and PAMAM (poly(amidoamine) dendrimers on the surface of the magnetite nanoparticles were confirmed with both TG and FT-IR. Due to the given saturation magnetization (M_s) of the products, they may be a powerful tool for biomedical applications and catalysis chemistry.

Keywords PAMAM · Dendrimers · SPION · Superparamagnetism

1 Introduction

Magnetite nanoparticles have attracted very much ineterest due to their unique important properties. They find application in the production of information storage materials, biomedical applications, catalysis reactions, and so on [1]. In order to prevent the agglomeration of magnetite nanoaparticles (attraction of nanoparticles due to the high saturation magnetization values of each nanoparticles), they are coated with some surfactants such as polymers, carboxylic acid, dendrimers, etc [2–5]. Therefore, these coated magnetite nanoparticles can be used in magnetic resonance imaging (MRI), drug delivery, cell separation, hyperthermia, etc. [6, 7].

The first dendritic structures that have been exhaustively investigated and have received widespread attention were Tomalia's poly(amidoamine) (PAMAM) dendrimer [8]. As it was stated by Yin et al. and others, PAMAM, a highly branched dendritic macromolecule having a unique surface with multiple chain ends, could also be used to modify the surface nanoparticles due to their good biocompatibility, highly geometric symmetry, chemical stability, controllable size, surface functionality, and adequate functional groups for chemical fixation [9–14]. PAMAM coating enables the reduction of particle agglomeration, and the terminal groups on the periphery can be tailored to control composite solubility [15]. Some important properties of these structures include a large number of end groups, the functionable cores, the nanoporous nature of the interior at higher generations, and easier crossing of biological barrier by transcytosis [16, 17]. Chandra et al. [18] demonstrated a facile approach for the preparation of dendrimers coated with Fe_3O_4 nanoparticles for drug delivery application.

In this study, the surface of amino silane-modified superparamagnetic iron oxide nanoparticles (SPION) was coated with polyamidoamine dendrimer up to the fifth generation, and their detailed structural, morphological, spectroscopic, and magnetic chracterizations were presented.

U. Kurtanm · S. Esir · A. Baykal (✉)
Chemistry Department, Fatih University, 34500 B. Çekmece, Istanbul, Turkey
e-mail: hbaykal@fatih.edu.tr

H. Sözeri
TUBITAK-UME, National Metrology Institute, P.O. Box 54, 41470, Gebze-Kocaeli, Turkey

2 Experimental

2.1 Chemicals

All chemicals were obtained from Merck and used as received without further purification.

2.2 Instrumentations

X-ray powder diffraction (XRD) analysis was conducted on a Rigaku Smart Lab Diffractometer operated at 40 kV and 35 mA using Cu Kα radiation ($\lambda = 1.54178$ Å).

Fourier transform infrared (FT-IR) spectra were recorded in transmission mode with a Perkin Elmer BX FT-IR infrared spectrometer. The powder samples were ground with KBr and compressed into a pellet (in the range 4,000–400 cm^{-1}).

Transmission electron microscopy (TEM) analysis was performed using a JEOL JEM 2100 microscope. A drop of diluted sample in alcohol was dripped on a TEM grid.

The thermal stability was determined by thermogravimetric analysis (TGA, Perkin Elmer Instruments model, STA 6000). The TGA thermograms were recorded for 5 mg of powder sample with a heating rate of 10 °C/min in the temperature range of 30–750 °C under nitrogen atmosphere.

VSM measurements were performed by using a Quantum Design Vibrating sample magnetometer (QD-VSM). The sample was measured between ± 10 kOe at room temperature and 10 K. Zero field cooling (ZFC) and field cooling (FC) measurements were carried out at 100 Oe, and the blocking temperature was determined from the measurements.

2.3 Procedure

2.4 Synthesis of SPIONs

Stoichiometric amounts of ferrous chloride hexahydrate ($FeCl_3 \cdot 6H_2O$, 99 %) and ferric chloride hexahydrate ($FeCl_2 \cdot 4H_2O$, 99 %) (with molar ratio of 2:1) were dissolved in 50 mL of distilled water. Ammonia solution (0.9 M) was used as alkaline source and vigorously stirred for 30 min and added to the above iron salt-containing solution till the pH of the solution reached to 11. After the addition of ammonia solution, the color of the iron salt-containing solution immediately turned to black. All experiments were done under Ar gas at room temperature. Finally, SPIONs were redispersed in an aqueous solution of tetramethylammonium hydroxide (TMAOH) (5 wt%).

2.4.1 Coating of SPIONs with Aminosilane

Fifty milliliters of the above solution (SPION in TMAOH soln) was mixed with 100 mL of ethanol in 250-mL two-necked bottom flask equipped with a condenser, and then

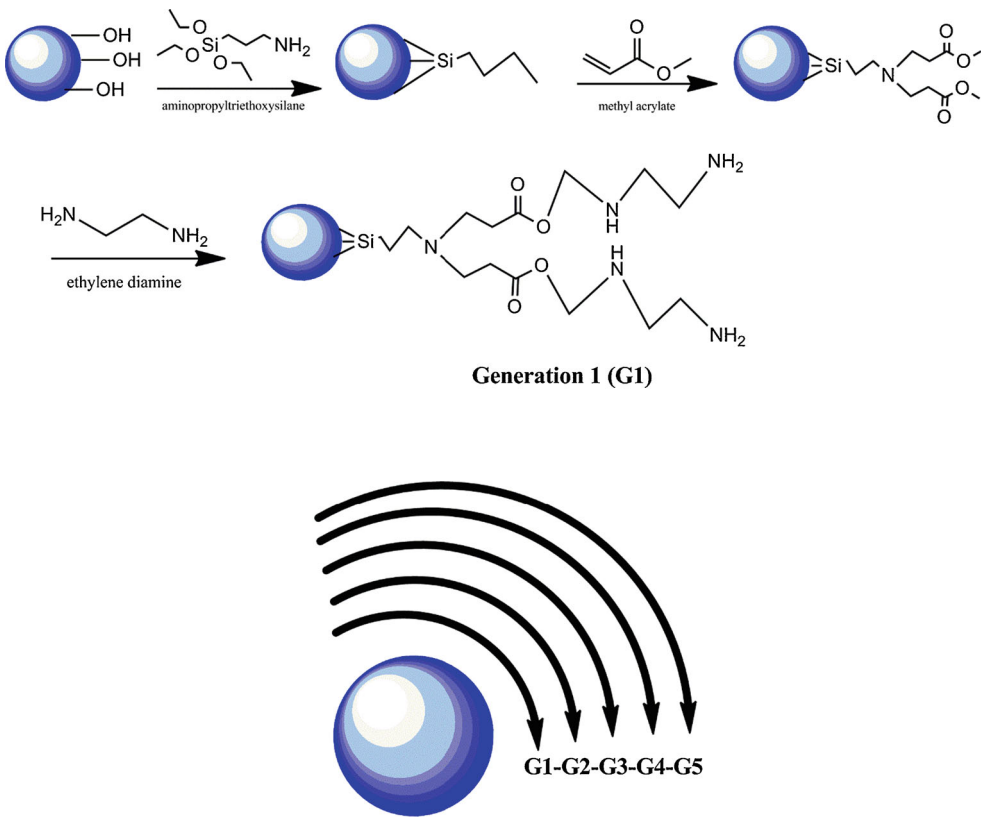

Scheme 1 Schematic representation of dendrimer-modified SPION-PAMAM G1 to G5

10 mL of 3-aminopropyltrimethoxysilane) (APTMS) was added under stirring at 60 °C for 12 h. Finally, the product was washed with ethanol and water several times by magnetic separation and dried under vacuum.

2.4.2 Synthesis of Dendrimer-Modified SPION–PAMAM G1 to G5

Ethylenediamine (10.0 g, 0.166 mol) was dissolved in 100 mL of methanol, and 94.6 g methyl acrylate was added to the above solution and stirred under nitrogen at 40 °C for 24 h. Excess methyl acrylate was removed under vacuum at room temperature. A Michael addition between the amine and the acrylate yielded a product bearing four terminal methyl ester groups. Subsequently, 120 g ethylenediamine was dissolved in methanol and added to the four-terminal methylester containing dendrimer and stirred for 48 h under nitrogen, and excess reactants were removed by vacuum distillation. Then a product bearing four terminal amino groups was obtained which was defined as the G1 PAMAM. By repeating the above cycle, a higher generation of PAMAM dendrimers (G2, G3, G4, G5) was synthesized. The purity of the amine-terminated PAMAM dendrimers was characterized via FT-IR. A schematic representation of dendrimer-modified SPION–PAMAM G1 to G5 was given in Scheme 1.

3 Results and Discussion

3.1 XRD Analysis

The XRD powder patterns of SPION–PAMAM G1 were presented in Fig. 1 which showed that the inorganic core is iron oxide (Fe_3O_4). The diffraction peaks were broadened owing to its small crystallite size. All observed diffraction peaks for five products could be indexed by the cubic structure of Fe_3O_4 well matched with the JCPDS no. 19-629 (only one XRD powder pattern was presented in this study). The line profile fitting method was used to estimate the crystallite size using Eq. 1 in Refs. [19] and [20]. The average crystallite size of the product was calculated by using line profile fitting as 4.2 ± 2.1 nm for the observed five peaks with the following Miller indices: (220), (311), (400), (511), and (440) [21].

3.2 FT-IR Analysis

The functionalization of SPION with aminosilane and PAMAM was monitored by FT-IR spectroscopy. Figure 2 shows the FT-IR spectra for uncoated SPION and PAMAM-coated SPION (dendrimer-modified SPION PAMAM G1 to G5). As it can be seen clearly from Fig. 2, Fe–O vibration peaks (which are due to the commercial magnetite powder: metal–oxygen band, ν_1, observed at 590 cm^{-1} corresponding to intrinsic stretching vibrations of the metal at a tetrahedral site ($Fe_{tetra} \leftrightarrow O$), whereas metal–oxygen band observed at 445 cm^{-1}, ν_2, is assigned to octahedral-metal stretching ($Fe_{octa} \leftrightarrow O$)) were observed for uncoated and all PAMAM-coated SPION. Additionally, organic vibration peaks were observed for all PAMAM-coated SPION (SPION PAMAM G1 to G5) [3, 22, 23]. The vibration of $-NH_2$ group was observed at 3,440 cm^{-1} in Fig. 2b–f. The stretching vibration of Si–O at the surface of aminosilane–Fe_3O_4 surface was about 990 cm^{-1}, which shifted to ~1,020 cm^{-1} of the SPION–PAMAM G5 due to the presence of highly electronegative –CO and $-NH_2$ groups [24, 25].

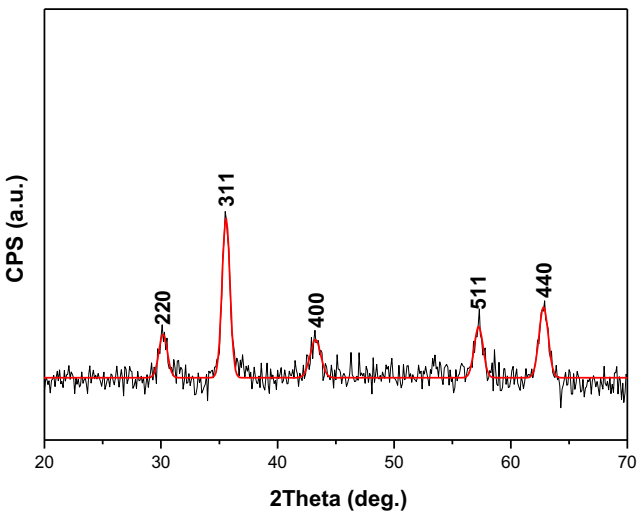

Fig. 1 XRD powder pattern and line profile fitting of dendrimer-modified SPION–PAMAM G1

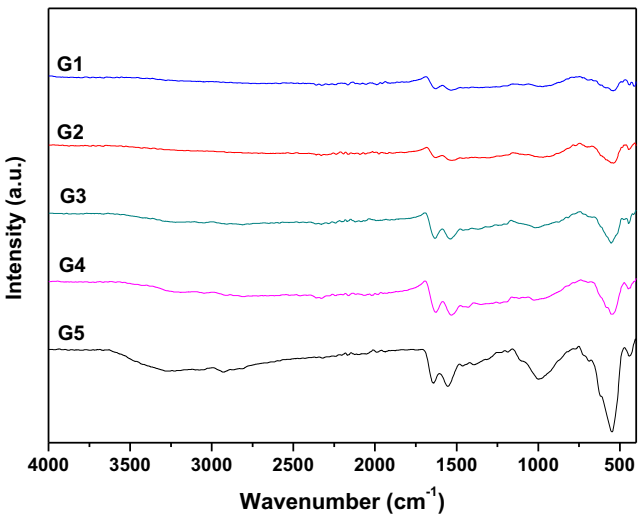

Fig. 2 FT-IR spectra of dendrimer-modified SPION–PAMAM G1 to G5

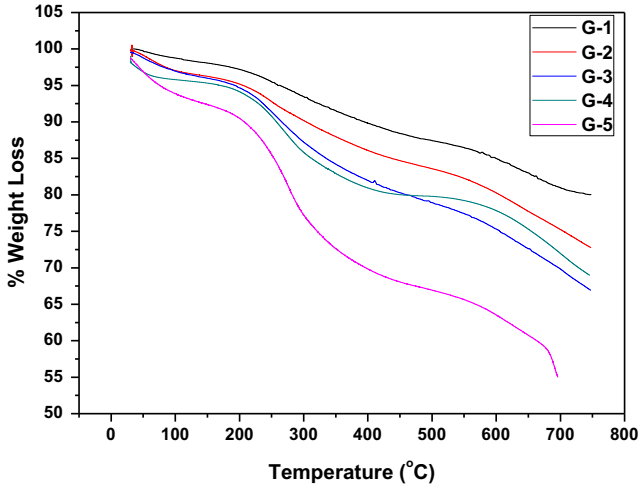

Fig. 3 TG thermogram of dendrimer-modified SPION–PAMAM G1 to G5

3.3 TG Analysis

The TG thermograms of dendrimer-modified SPION–PAMAM G1 to G5 were presented in Fig. 3. As in the case of the previous studies related to synthesis of PAMAM dendrimer, TGA results of this study are similar [2, 26–30]. The percent of weight loss was increased with increasing dendrimer generation number as expected due to the increase in the chain length of C-backbone and molecular weight of dendrimers. The weight loss of each product (dendrimer-modified SPION–PAMAM G1 to G5) was given in Table 1.

3.4 TEM Analysis

In order to investigate the morphology and particle size distribution of the dendrimer-modified SPION–PAMAM G1 to G5, TEM analysis was done. The TEM images and their particle size distribution diagrams for each product were given in Fig. 4, respectively. As the generation number was increased, the particle size of the related product was also increasing accordingly (SPION–PAMAM from G1 to G5). A nearly spherical morphology was observed for TEM images of all products, while some other polygonic morphologies were also observed as stated by Uzun et al. [3] and Mikhaylova et al. [24]. Due to the magnetic dipole–dipole interaction and high surface to volume ratio of all products, some degree of agglomeration were observed [24, 31]. In order to analyze the size distribution quantitatively, the particle size distribution was fitted using a log-normal function [32]:

$$P(D) = \frac{A}{D\sigma_D\sqrt{2\pi}} \exp\left(-\frac{1}{2\sigma_D^2}\ln^2\left(\frac{D}{D_O}\right)\right) \quad (1)$$

where σ_D is the standard deviation of the diameter, and D_0 is the mean diameter.

3.5 VSM Analysis

Room-temperature magnetization curves of the dendrimer-modified SPION–PAMAM G1 to G5 were given in Fig. 5. The saturation magnetization (M_s) values of the samples were derived from the plot of M vs. 1/H as shown in Table 1 Magnetization of the composites decreases regularly with increasing number of dendrimer generation due to the presence of a nonmagnetic layer at the particle surface and spin canting [2, 23]. All M_s values are lower than the theoretical value of bulk magnetite (i.e., 92 emu/g) [33, 34]. Besides, all M–H hysterisis curves have no remanence and no coercivity with the absence of saturation at high fields. These features are typical characteristics of superparamagnetic (SP) nanoparticles and can be described well with the Langevin theory of magnetization. Accordingly, the magnetization of SP nanoparticles varies with the external field as follows:

$$M = M_s\left\{\mathrm{Coth}\left(\frac{\mu H}{k_B T}\right) - \frac{k_B T}{\mu H}\right\}, \quad (2)$$

where μH represents the energy due to the external field, and $k_B T$ stands for the thermal energy. The mean magnetic moment, μ, is related to the average particle size and can be calculated by fitting the above equation to measured M–H hysterisis curves. Thus, the average sizes of the magnetic cores of SPIONs coated with PAMAM dendrimes are around 9 nm. Despite a small discrepancy with TEM observations, all the measured or calculated grain sizes are below the superparamagnetic limit of 20 nm for magnetite [35–37].

Table 1 Particle size and weight loss of dendrimer-modified SPION–PAMAM G1 to G5

Product	Particle size (nm)	Weight loss (%)	M_s(emu/g)
SPION–PAMAM G1	4.4 ± 2.0	20	54.1
SPION–PAMAM G2	4.9 ± 2.1	27	48.8
SPION–PAMAM G3	6.2 ± 2.3	31	45.1
SPION–PAMAM G4	8.5 ± 2.1	34	43.3
SPION–PAMAM G5	9.1 ± 2.0	41	37.6

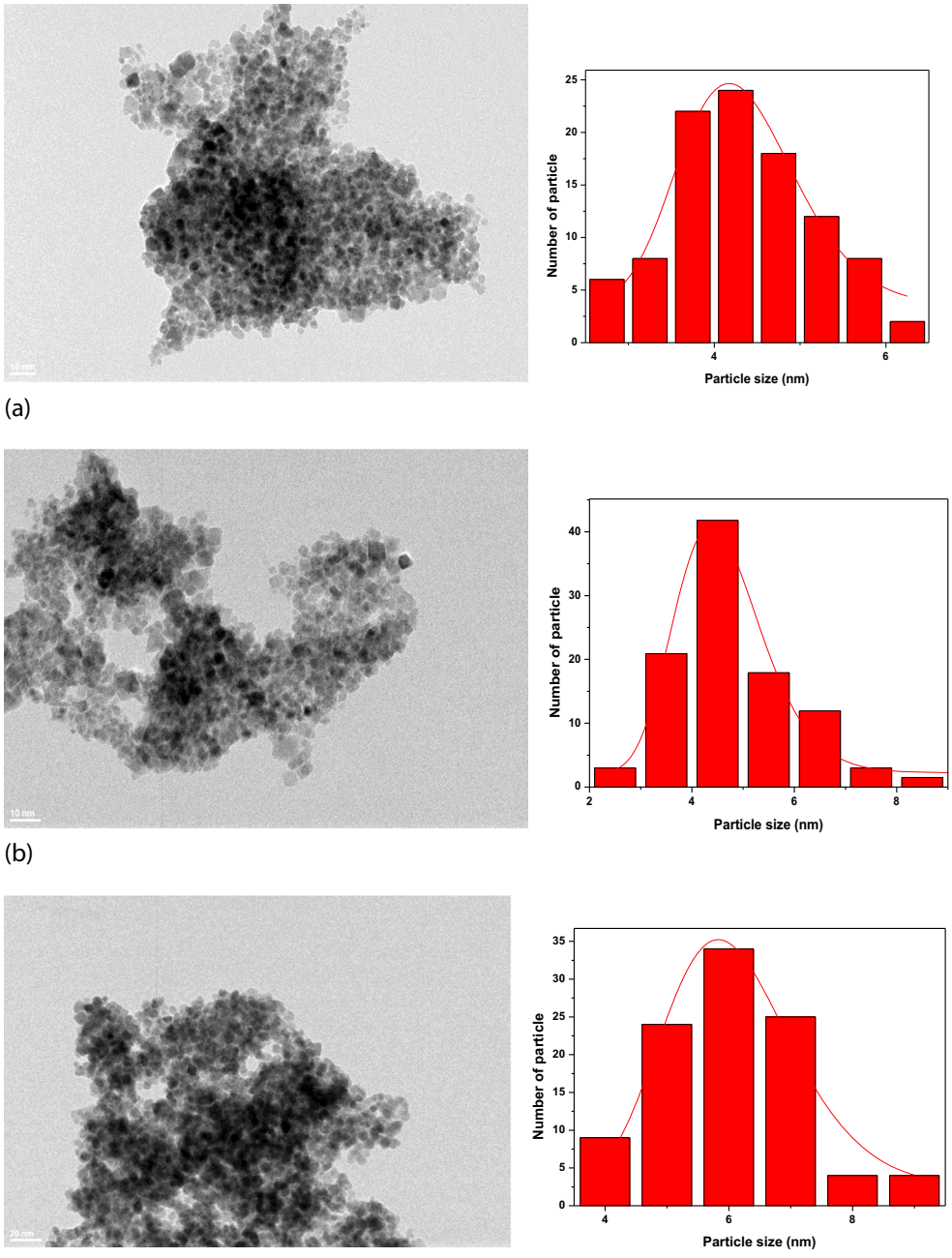

Fig. 4 TEM micrographs and particle size distribution diagrams of dendrimer-modified SPION–PAMAM: **a** G1, **b** G2, **c** G3, **d** G4, and **e** G5

Fig. 4 (continued)

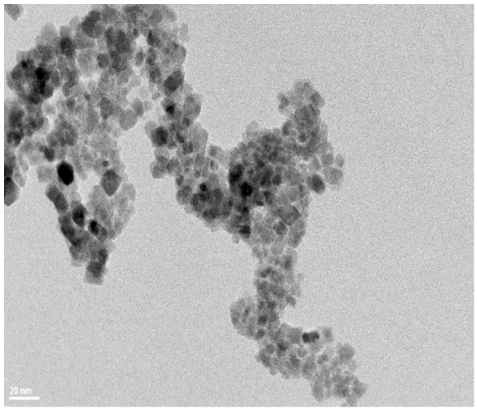

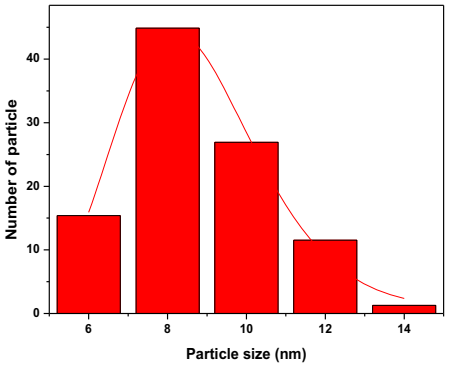

(d)

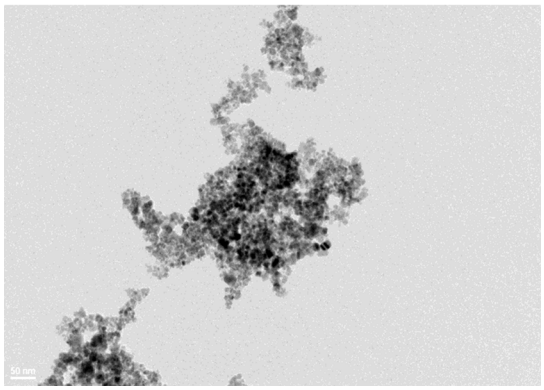

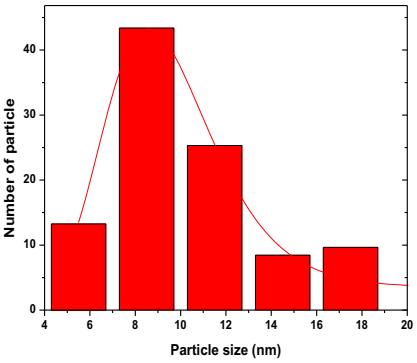

(e)

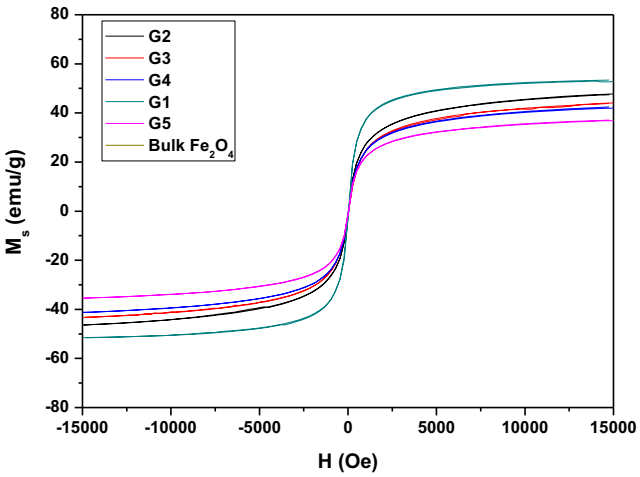

Fig. 5 Room temperature M–H curve of bulk Fe_3O_4 NPs and dendrimer-modified SPION–PAMAM (G1, G2, G3, G4, and G5)

4 Conclusion

In this study, APTMS was grafted onto the surface of magnetite nanoparticles which were then used for successive addition of methyl acrylate and ethylenediamine step by step to form dendritic structure of PAMAM on the SPION. Dendrimer-modified SPION–PAMAM G1 to G5 with considerable magnetic properties were synthesized. The presence of PAMAM generations on the surface of the magnetite was confirmed with FT-IR, TEM, and TGA. Crystallite, particle, and magnetic core sizes are consistent with each other. All products present superparamagnetic property. As a further study, the synthesized products will be used for protein separation and hydrogen reactions as magnetically recyclable catalyst.

Acknowledgments This work was supported by Fatih University under BAP grant no. P50021301-Y (3146).

References

1. Hong, R., Hi, J., Wang, J., Li, H.: China Particuol **5**, 186–191 (2008)
2. Tajabadia, M., Khosroshahia, M.E., Bonakdar, S.: Colloids Surf. A Physicochem. Eng. Asp **431**, 18–26 (2013)
3. Uzun, K., Çevik, E., Şenel, M., Sözeri, H., Baykal, A., Abasıyanık, M.F., Toprak, M.S.: J. Nanopart. Res. **12**, 3057–3067 (2010)
4. Durmus, Z., Sözeri, H., Unal, B., Baykal, A., Topkaya, R., Kazan, S., Toprak, M.S.: Polyhedron **30**, 322–328 (2011)

5. Garlyyev, B., Durmus, Z., Kemikli, N., Sozeri, H., Baykal, A., Ozturk, R.: Polyhedron **30**, 2843–2848 (2011)
6. Zhano, D.L., Zheng, X.W., Xi, O.S., Tang, J.T.: J. Alloys Compd. **469**, 215–222 (2009)
7. Racuciu, M., Creang, D.E., Airinei, A.: Eur. Phys. J. **E21**, 117–121 (2006)
8. Kesharwani, P., et al.: Dendrimer asnanocarrier fordrugdelivery. Prog. Polym. Sci. http://dx.doi.org/10.1016/j.progpolymsci.2013.07.005 (2013)
9. Takada, K., Abruña, H.: J. Electroanal. Chem. **567**, 249–256 (2004)
10. Yin, H., Cui, L., Chen, Q., Shi, W., Ai, S., Zhub, L., Lu, L.: Food Chem **125**, 1097–1103 (2011)
11. Krämer, M., Perignon, N., Hagg, R., Marty, J.D., Thomann, R., Viguerie, N.L., Migotand, C.: Macromolecules **38**, 8308–8312 (2005)
12. Tomalia, D.A., Baker, H., Dewald, J., Hall, M., Kallos, G., Martin, S., Roeck, J., Ryder, J., Smith, P. Polym. J. **17**, 117–125 (1985)
13. Gaofei, D., Yan, S., Zhifeng, F.U., Wantai, Y.: Chin. J. Catal. **33**, 651–658 (2012)
14. Gao, F., Pan, B.F., Zheng, W.M., Ao, L.M., Gu, H.C.: J. Magn. Magn. Mater. **293**, 48 (2005)
15. Crooks, R.M., Zhao, M., Sun, L., Chechik, V., Yeung, L.K.: Acc. Chem. Res. **34**, 181–187 (2001)
16. Peng, X., Pan, Q., Rempel, G.L.: Chem. Soc. Rev. **37**, 1619–1628 (2008)
17. Antharjanam, P.K.S., Jaseer, M., Ragi, K.N., Prasad, E.: J. Photochem. Photobiol. A **203**, 50–55 (2009)
18. Chandra, S., Mehta, S., Nigam, S., Bahadur, D.: New J. Chem. **34**, 648–655 (2010)
19. Wejrzanowski, T., Pielaszek, R., Opalińska, A., Matysiak, H., Lojkowski, W., Kurzydlowski, K.J.: Appl. Surf. Sci. **253**, 204–209 (2006)
20. Pielaszek, R.: Appl. Crystallography Proceedings of the XIX Conference, Krakow, Poland, 43 (2003)
21. Qie, F., Zhang, G., Houa, J., Sun, X., Luoa, S., Tan, T.: Talanta **93**, 166–171 (2012)
22. Wei, S., Zhu, Y., Zhang, Y., Xu, J. React. Funct. Polym. **66**, 1272–1277 (2007)
23. Bruce, I.J., Taylor, J., Todd, M., Davies, M.J., Borioni, E., Sangregorio, C., Sen, T.: J. Magn. Magn. Mater. **284**, 145–160 (2004)
24. Mikhaylova, M., Kim, D.K., Berry, C.C., Zagorodni, A., Toprak, M., Curtis, A.S.G., Muhammed, M.: Chem. Mater. **16**, 2344–2354 (2004)
25. Toprak, M.S., McKenna, B.J., Waite, H., Stucky, G.D.: Chem. Mater. **19**, 4263–4269 (2007)
26. Kavas, H., Durmus, Z., Tanrıverdi, E., Senel, M., Sozeri, H., Baykal, A.: J. Alloys Compd **509**, 5341–5348 (2011)
27. Shi, X., Wang, S.H., Shen, M., Antwerp, M.E., Chen, X., Li, C., Petersen, E.J., Huang, Q., Weber, W.J., Baker, J.R. Biomacromolecules **10**, 1744–1750 (2009)
28. Baykal, A., Toprak, M.S., Durmus, Z., Senel, M., Sozeri, H., Demir, A.: J. Supercond. Nov. Magn. **25**, 1541–1549 (2012)
29. Qie, F., Zhang, G., Houa, J., Sun, X., Luoa, S., Tan, T. Talanta **93**, 166–171 (2012)
30. Pan, B.F., Gao, F., Gu, H.C.: J. Colloid Interf. Sci. **284**, 1–6 (2005)
31. Tomalia, D.A., Naylor, A.M., Goddard, W.A.: Vol. 29, pp. 138–175 (1990)
32. Kim, T., Shima, M.: Vol. 101, pp. 09M516–09M522 (2007)
33. Faiyas, A.P.A., Vinod, E.M., Joseph, J., Ganesan, R., Pandey, R.K.: J. Magn. Magn. Mater. **322**, 400–404 (2010)
34. Cullity, B.D.: Introduction to Magnetic Materials, 61, 190–196 (1972)
35. Kodama, R.H., Berkowitz, A.E., McNiff, E.J., Foner, S.: Phys. Rev. Lett. **77**, 394–400 (1996)
36. Batlle, X., Labarta, A.: J. Phys. D: Appl. Phys. **35**, R15–R42 (2002)
37. Mürbe, J., Rechtenbach, A., Töpfer, A.: Mat. Chem. Phys. **110**, 426–433 (2008)